Journal of Power Sources 241 (2013) 709–717

Contents lists available at SciVerse ScienceDirect

Journal of Power Sources

journal homepage: www.elsevier.com/locate/jpowsour

Electrospun carbon nanofibres as electrode materials toward VO^{2+}/VO_2^+ redox couple for vanadium flow battery

Guanjie Wei, Jianguo Liu, Huan Zhao, Chuanwei Yan*

State Key Laboratory for Corrosion and Protection, Institute of Metal Research, Chinese Academy of Sciences, Shenyang 110016, China

HIGHLIGHTS

- The ECNFs were firstly used as electrode materials for VFB in this paper.
- Evolution of nitrogen functional groups helps to the graphitization of ECNFs.
- Forming of the 2-dimensional graphitic lattice improves the activity of ECNFs.
- Compared with the TCFs, ECNFs exhibit higher activity toward VO^{2+}/VO_2^+ couple.

ARTICLE INFO

Article history:
Received 26 January 2013
Received in revised form
12 April 2013
Accepted 1 May 2013
Available online 18 May 2013

Keywords:
Electrospinning
Polyacrylonitrile
Carbon nanofibres
Electrode
Vanadium flow battery

ABSTRACT

Polyacrylonitrile (PAN) carbon nanofibres with diameters of 100–200 nm have been developed by electrospinning and subsequent carbonization process. The composition, structure, electrical conductivity, and electrochemical properties of the carbon nanofibres as electrode materials for vanadium flow battery (VFB) have been characterized. It is found that with the increasing of carbonization temperature, the electrochemical activity of carbon nanofibres toward VO^{2+}/VO_2^+ redox couple is enhanced greatly. Particularly, the 1000 °C-carbonized nanofibres show excellent performance. The good behavior of the nanofibres carbonized at high temperature may attribute to the conversion of fibers inner-structure and the improvement of electrical conductivity. Compared with the traditional carbon fibers (TCFs), electrospun carbon nanofibres (ECNFs) carbonized at temperature of 1000 °C exhibit higher activity toward the vanadium reaction, presenting considerable potential for electrode application in VFB.

1. Introduction

With the fast development of renewable energy (wind energy and solar energy), the demand for technology of energy conversion and storage has become much stronger than ever [1–3]. As a large scale energy storage system, VFB has attracted extensive attention recently, due to its long cycle life, large capacities, flexible operation, and low cost [4–6]. In the VFB system, electrodes play an important role, and carbon-based materials such as carbon felt [7], carbon paper [8], and graphite powder [9,10] are used as typical electrodes in VFB. Though advantages of these materials are various, including high surface area, wide operating potential range, good stability, and reasonable cost [11–13], the poor kinetics and reversibility of them limit their use in VFB. For this reason, much attention has been paid to modify the electrode materials to enhance their electrochemical activities. Many methods are widely used, such as thermal treatment [14], acid oxidation [15,16] and metal deposition [17,18]. By modulating the surface properties of carbon materials especially introducing oxygen functional groups onto their surface, these methods are aimed at lowering the activation barrier of the vanadium reaction and improving the reaction rate. However, the effect of modification in these methods is limited and is not durable. In this regard, developing a new kind of carbonaceous electrode material and investigating the effect of their morphology, composition, structure, and electrical conductivity on electrochemical properties toward vanadium couples systematically are in a dire need.

Currently, electrospinning has emerged as an efficient and inexpensive approach to prepare carbon nanofibres and high surface area fibrous membrane. This promising technique has been extensively explored in energy field especially in the supercapacitor [19,20] and lithium-ion battery [21,22]. However, the ECNFs have not been used in VFB yet. Arshad et al. [23] reported that the inner-structure of carbonized PAN nanofibres strongly depends on the

* Corresponding author. Tel.: +86 24 2399 8320; fax: +86 24 2388 0201.
E-mail address: cwyan@imr.ac.cn (C. Yan).

0378-7753/$ – see front matter © 2013 Elsevier B.V. All rights reserved.
http://dx.doi.org/10.1016/j.jpowsour.2013.05.008

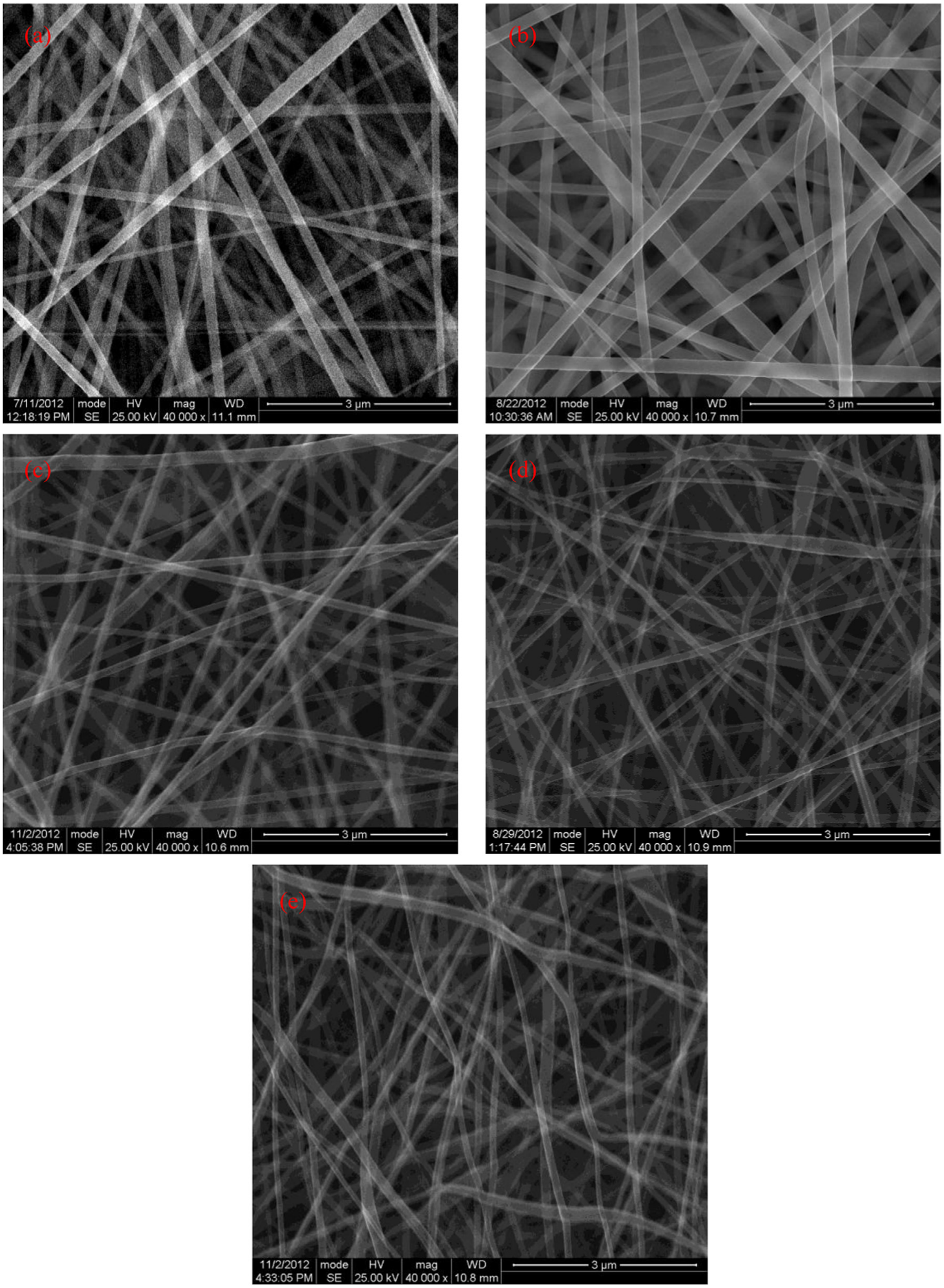

Fig. 1. Surface morphology of PAN nanofibres: (a) the electrospun nanofibres, (b) the pre-oxidized nanofibres, (c) the 750 °C-carbonized nanofibres, (d) the 800 °C-carbonized nanofibres, (e) the 1000 °C-carbonized nanofibres.

carbonization temperature. In this paper, the PAN nanofibres were developed by electrospinning technique firstly, and then the nanofibres were carbonized at different temperature to prepare the ECNFs. After that, the ECNFs were used as electrode materials for VFB. The conversion of the carbon nanofibres inner-structure and the improvement of electrical conductivity relating to the carbonization temperature were studied, and their effect on the electrochemical properties was also investigated. In addition, the

electrochemical properties of ECNFs were compared with that of TCFs by modifying the glass carbon electrode (GCE).

2. Experimental

2.1. Electrode preparation

ECNFs were prepared by process of electrospinning, pre-oxidation, and carbonization. 10 wt.% of PAN was dissolved in *N*,*N*-dimethylformamide (DMF) by stirring at 60 °C for 4 h to prepare the precursor solution for electrospinning. The electrospinning was carried out at a positive direct current voltage of 25 kV. The precursor solution was placed in a 10 mL plastic syringe with a metal needle of 0.84 mm diameter and derived by a syringe pump at a flow rate of 1.4 mL h^{-1}. The electrospun nanofibres were collected by a roller at a rotating speed of 200 r min^{-1} and the distance between the needle and the collector was 20 cm. Then the electrospun nanofibres were pre-oxidized at 280 °C for 30 min in air. After that, the stabilized nanofibres were carbonized by heating them to 600 °C, 700 °C, 750 °C, 800 °C, 900 °C, and 1000 °C at a rate of 5 °C min^{-1} and holding for 30 min in nitrogen flow. After this process, the ECNFs were obtained.

2.2. Materials characterizations

The surface morphology and diameter distribution of ECNFs were examined by FEI INSPECT F scanning electron microscopy (SEM). The surface elements and functional groups of the nanofibres were analyzed by X-ray photoelectron spectroscopy (XPS). All binding energy values were calibrated to the C1s graphitic peak at 284.7 eV. The conversion of carbon structure was reflected by Raman spectra. The microstructure of the carbon nanofibres was studied by X-ray diffraction (XRD) and transmission electron microscopy (TEM). The electrical conductivity of the samples was measured by the four-probe method.

2.3. Cyclic voltammetry measurement

For cyclic voltammetry (CV) measurement, a three-electrode cell was used with the fibrous membrane made up of ECNFs as the working electrode, a saturated calomel electrode as the reference electrode, and a Pt electrode as the counter electrode. The working electrode was produced by sandwiching a piece of membrane between a rubber sheet and a Ti plate. The sheet had a hole of 1.286 cm^2 as the working area, and the Ti plate contacting the membrane directly acted as current collector. The measurement was performed in 0.1 M $VOSO_4$ + 2.0 M H_2SO_4 solution.

2.4. Loading of carbon fibers on the GCE

Both of the electrospun fibrous membrane and the PAN-based carbon felt (Shenhe carbon fiber Materials Co. Ltd) were ground up by an agate mortar to obtain the discrete ECNFs and TCFs. Then the two kinds of carbon fibers (each for 4 mg) were added into the 1 mL DMF under ultrasonication, respectively. When the carbon fibers were well dispersed and suspended in the solution, 20 uL suspension was dropped onto the surface of GCE (diameter: 5 mm) and dried at 80 °C for 2 h. After that, the GCE coated by carbon fibers was tested by CV and electrochemical impedance spectra (EIS) measurement. The CV curves were recorded at 10 mV s^{-1} scan rate. The EIS was measured by applying an alternating voltage of 5 mV over the frequency ranging from 10^5 Hz to 10^{-2} Hz. The measurement area of samples is 0.196 cm^2. The GCE without loading of carbon fibers was also tested as comparison.

Table 1
Elements content of the ECNFs at the different carbonization temperature.

Elements	600 °C (%)	700 °C (%)	750 °C (%)	800 °C (%)	900 °C (%)	1000 °C (%)
C	81.65	83.42	83.52	88.23	90.93	92.61
N	11.11	9.24	12.00	5.57	3.76	3.97
O	7.16	7.34	4.24	6.10	4.78	3.00
S	0.09	0	0.24	0.09	0.53	0.43

3. Results and discussion

3.1. SEM images

The morphology of electrospun nanofibres, pre-oxidized nanofibres, and carbonized nanofibres is shown in Fig. 1. Most of the nanofibres have a smooth surface and uniform crosssection, though fusiform droplets appear in some cases. Compared with the electrospun and pre-oxidized nanofibres, most of the carbonized nanofibres look benter and thinner. This may attribute to the volume shrinkage of PAN due to the weigh loss during the carbonization [21]. Compare the morphology of nanofibres carbonized at different temperature, the diameters of the carbon nanofibres are not changed significantly and are distributed with the range of 100–200 nm. Besides, during the pre-oxidation process, the electrospun nanofibres undergo a change in color from white to dark brown as the previous work reported [24]. The mechanism for this phenomenon has not been fully understood yet.

3.2. XPS analysis

In order to identify the composition of the ECNFs carbonized at the different temperature, XPS analysis is used. Table 1 presents the elements of the ECNFs which mainly include carbon, nitrogen, and oxygen. The change of the elements content is illustrated in Fig. 2. With the increasing of the carbonization temperature, the carbon content increases while the nitrogen and oxygen content decrease. This tendency is in accordance with the rule of PAN carbonization.

Fig. 3 shows the curve-fitted N1s high-resolution XPS of the ECNFs at the different carbonization temperature. The optimum fitting was achieved by resolving each N1s spectrum into four peaks [25,26]. Peak I (398.0–398.2 eV) corresponds to the pyridinic nitrogen; Peak II (399.1–399.8 eV) to the pyrrolic nitrogen; Peak III (400.2–400.9 eV) to the graphitic nitrogen and Peak IV centering around 402.0 eV may be assigned to the Pyridine N-oxide. The respective percentage of the nitrogen functional groups is listed in Table 2.

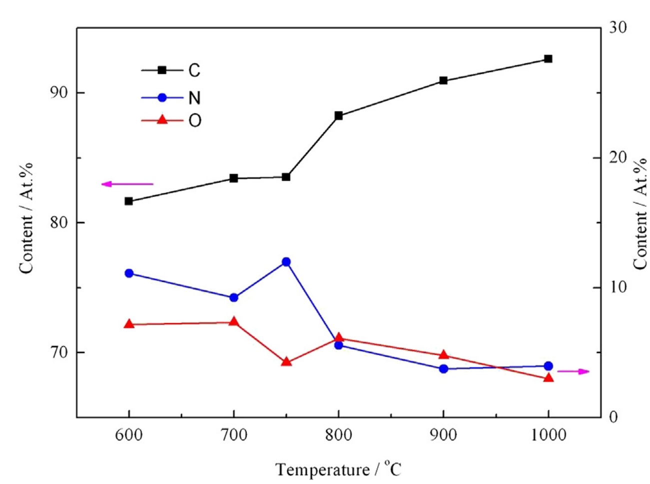

Fig. 2. Change of the elements content in the ECNFs.

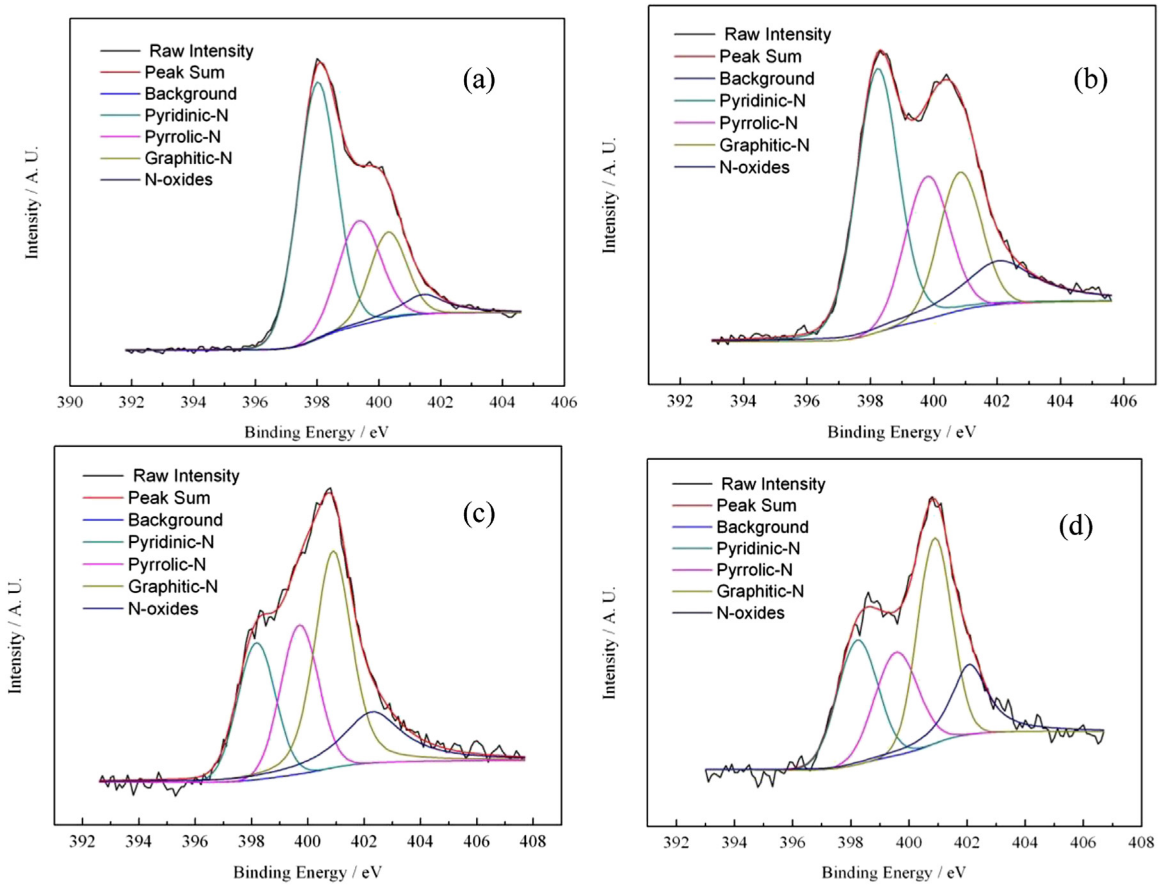

Fig. 3. Curve-fitting of the N1s high-resolution XPS from the ECNFs at the different carbonization temperature: (a) 700 °C, (b) 800 °C, (c) 900 °C, (d) 1000 °C.

Fig. 4 illustrates the evolution of nitrogen functional groups during the carbonization process. It can be seen clearly that with the increasing of carbonization temperature, the content of pyridinic nitrogen decreases significantly while that of graphitic nitrogen and pyridine N-oxide increase accordingly. The content of pyrrolic nitrogen remains more or less constant over the complete temperature range up to 1000 °C. During the pre-oxidation process, the acrylonitrile moieties form a "ladder" structure due to the cyclization of the cyano groups. With the low-temperature carbonization further, hydrogen may be released and a series of pyridine rings can be formed [25]. Therefore, pyridinic nitrogen is the most abundant nitrogen functional groups at low carbonization temperature such as 600 °C, 700 °C and 750 °C. Upon carbonized at higher temperature, the "ladder" structure present in the ECNFs crosslinks and forms a 2-dimensional graphitic lattice [26]. Consequently, the relative content of the pyridinic nitrogen is drastically reduced and the graphitic nitrogen becomes the dominating nitrogen functional groups, a process which is accompanied by a strong decrease of the total nitrogen content. Fig. 4 also indicates that the evolution of nitrogen functional groups mainly happens in the carbonization temperature range from 750 °C to 900 °C.

The O1s high-resolution XPS reveal the presence of three peaks [27–29]. Peak I (530.8–531.1 eV) corresponds to C=O groups (ketone, lactone, carbonyl), Peak II (531.7–532.3 eV) to carbonyl oxygen atoms in esters, amides, carboxylic anhydrides and oxygen atoms in hydroxyls or ethers, and Peak III (533.1–533.5 eV) probably to chemisorbed oxygen or adsorbed water. The respective percentage of the oxygen functional groups is listed in Table 3. Compared with the nitrogen functional groups, evolution of the oxygen functional groups is less apparently particularly inside the temperature range from 750 °C to 900 °C [30]. At the carbonization temperature of 1000 °C, the oxygen functional groups change a lot, for some of them may decompose [31].

3.3. Raman analysis

Raman scattering is an effective technique for probing the structure of the carbonaceous materials. Fig. 5 shows the Raman spectra of the ECNFs. Two characteristic peaks were observed in the samples. The so-called G band centers around 1580 cm^{-1} and the D band centers around 1350 cm^{-1}. The G band is commonly observed in the ideally ordered graphitic structure, corresponding to the stretching vibration mode with E_{2g} symmetry in the aromatic layers of the crystalline graphite [32]. The D band is usually called the defect band, which is ascribed to the disordered graphitic lattice such as the defects, heteroatoms and edge planes [33]. The intensity area ratio of D band and G band (I_D/I_G) and the width of the

Table 2
Percentage of the nitrogen functional groups for ECNFs at the different carbonization temperature.

Nitrogen groups	600 °C (%)	700 °C (%)	750 °C (%)	800 °C (%)	900 °C (%)	1000 °C (%)
Pyridinic N	50.9	53.1	49.5	41.5	20.8	25.0
Pyrrolic N	22.5	23.1	21.2	22.0	22.7	22.2
Graphitic N	18.7	17.1	19.9	20.2	37.9	35.2
Pyridine N-oxide	7.8	6.7	9.4	16.4	18.5	17.6

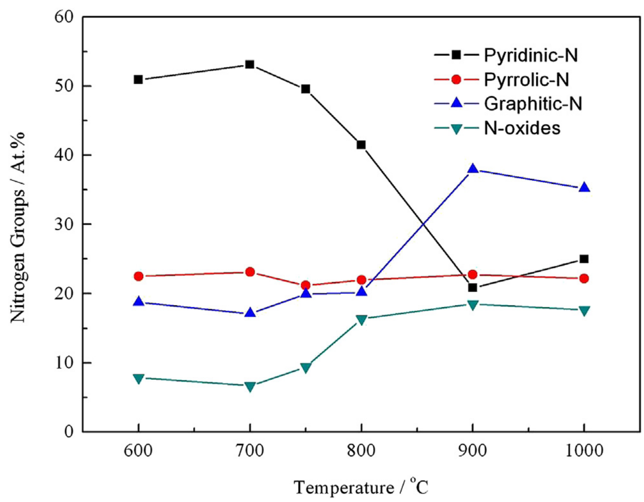

Fig. 4. Evolution of the nitrogen functional groups at the different carbonization temperature.

two bands have been proved to have good correlations with the degree of carbon structural order. Tuinstra and Knight [34,35] have reported that the lateral graphitic crystallite size La can be calculated by I_D/I_G as following equation:

$$La/nm = 4.4 * I_G/I_D$$

The relative parameters are listed in Table 4.

With the increasing of carbonization temperature, the width of the two bands and the I_D/I_G decrease obviously, indicating the graphitization degree of the ECNFs enhances a lot. At the same time, the lateral crystallite size La enlarges from 1.7 nm to 2.7 nm in the temperature range of 700–900 °C, which shows good agreement with the other previous work [36]. However, when the carbonization temperature was raised upto 1000 °C, graphitization degree of the ECNFs has not improved as previously noted, though the C element content increases. Combining the result with the XPS analysis mentioned above, it can be found that evolution of the nitrogen functional groups mainly happens in the temperature range from 750 °C to 900 °C. The conversion from pyridinic nitrogen to graphitic nitrogen contributes to the forming of the 2-dimensional graphitic lattice. Therefore, as the carbonization temperature was raised upto 900 °C, the degree of carbon structural order and the graphite crystallite size of the ECNFs improve extensively, and accordingly, the relative aspects have not been promoted further at the temperature of 1000 °C.

3.4. XRD analysis and TEM images

The XRD curve in Fig. 6 reflects the crystal structure of the 1000 °C-carbonized nanofibres. The carbon nanofibres exhibit a 3-dimensional diffraction peak around 23.7°, which corresponds to the (002) crystallographic plane of the graphite crystallites. Compared to the (002) diffraction peak of the graphite, the peak in the ECNFs is so broad and shifts significantly toward lower 2θ, indicating that graphitization of the ECNFs is very poor. The d_{002} value of the ECNFs (0.375 nm) calculated by Bragg formula is larger than that of graphite (0.335 nm), implying that the microstructure of ECNFs is a turbostratic carbon structure [37]. The peak located around 43° with low intensity corresponds to the (10) crystallographic plane of the 2-dimensional graphitic lattice [24,38]. These all observations demonstrate the graphitization degree of the ECNFs is very low even at high carbonization temperature of 1000 °C.

In order to examine the microstructure of the ECNFs further, TEM images of the 1000 °C-carbonized nanofibres are obtained. As shown in Fig. 7, a series of elongated graphite crystallites is aggregated and generally aligned along the fiber axis. However, the ordered graphite layers are not observed in the high-resolution TEM image of the nanofibres. Therefore, the turbostratic structure in the nanofibres may be viewed as 2-dimensional polycrystals with a preferred orientation in parallel to the fiber axis [39,40]. Because the electrospun nanofibres are collected by a rotating roller in the experiment, the polyacrylonitrile will be pulled in the direction of rotation and aligned along the fiber axis more or less during the electrospinning process. The following steps such as cyclization of the cyano groups and the crosslinking of the “ladder” structure will also take place in situ. These may give rise to the preferred orientation of the 2-dimensional graphitic lattice.

Table 3
Percentage of the oxygen functional groups for ECNFs at the different carbonization temperature.

Oxygen groups	600 °C (%)	700 °C (%)	750 °C (%)	800 °C (%)	900 °C (%)	1000 °C (%)
C=O	51.3	52.6	46.3	45.4	45.7	25.4
C–O	31.7	30.3	27.4	27.8	30.0	37.7
Adsorbed water	16.9	17.2	26.3	26.8	24.3	36.9

3.5. Electrical conductivity

Fig. 8 shows the electrical conductivity of the ECNFs. The relative data are listed in Table 5. Due to the extremely poor electrical conductivity, resistance of the 600 °C-carbonized nanofibres is beyond the measurement range. With the increasing of the carbonization temperature, the electrical conductivity of the ECNFs improves a lot especially in the temperature range from 750 °C to 900 °C. The result is in keeping with the evolution of the nitrogen functional groups and the transition of the carbon structure. It indicates that the electrical conductivity of the ECNFs strongly depends on their graphitization degree. Compared with the 900 °C-carbonized nanofibres, the electrical conductivity of the 1000 °C-carbonized nanofibres increases a little, which may due to the further increase of the C element content.

3.6. CV behavior

As illustrated in Fig. 9, CV behavior of the ECNFs carbonized at different temperature was investigated at scan rate of 2 mV s^{-1} in the electrolyte containing 0.1 M $VOSO_4$ and 2 M H_2SO_4. The electrochemical parameters are listed in Table 6. In the case of the ECNFs carbonized at the temperature lower than 800 °C, the two peaks corresponding to the oxidation of VO^{2+} to VO_2^+ and the reduction of VO_2^+ to VO^{2+} are not clear, implying that it is of low electrochemical activity on these samples. The 800 °C-carbonized nanofibres present a better electrochemical property, as the voltammogram shows a couple of peaks obviously corresponding to the VO^{2+}/VO_2^+ redox reaction.

However, in comparison with the first few samples, a dramatic increase in the electrochemical property happens to the 900 °C-carbonized nanofibres. As shown in Table 6, the 900 °C-carbonized nanofibres exhibit the highest anodic and cathodic peak current, reflecting the huge improvement in electrochemical activity toward the VO^{2+}/VO_2^+ redox couple. At the same time, the reversibility of the redox couple also becomes better on the 900 °C-carbonized nanofibres, since the sample has smaller peak potential separation accompanied by a ratio of peak current (Ipa/Ipc) closed to unity. The excellent performance can attribute to the conversion

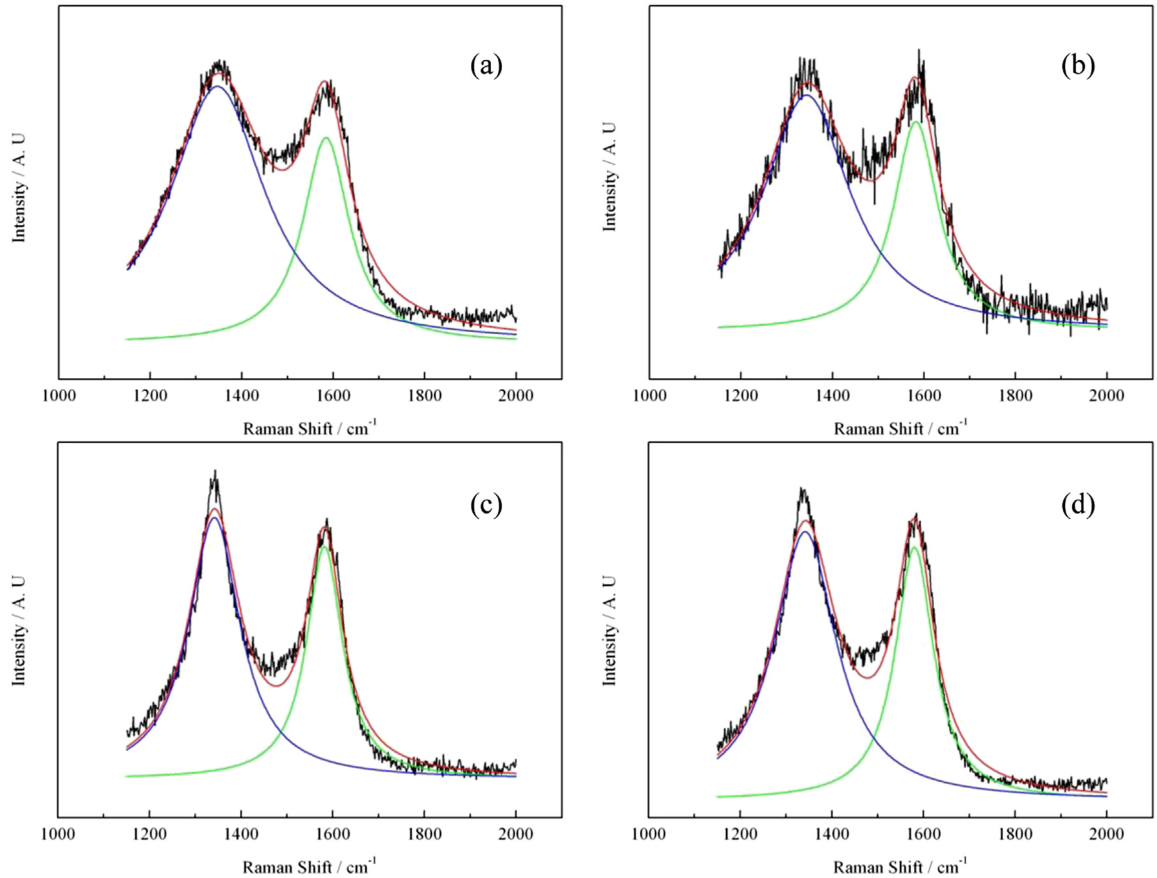

Fig. 5. Raman spectra of the ECNFs at the different carbonization temperature: (a) 700 °C, (b) 800 °C, (c) 900 °C, (d) 1000 °C.

Table 4
Parameters obtained from Raman spectra for the ECNFs at the different carbonization temperature.

Temperature (°C)	D band		G band		I_D/I_G	La (nm)
	Center (cm^{-1})	Width (cm^{-1})	Center (cm^{-1})	Width (cm^{-1})		
700	1346.9	250.5	1584.3	123.6	2.5	1.7
800	1343.4	229.2	1582.3	118.8	2.2	2.0
900	1341.5	136.6	1581.7	95.6	1.6	2.7
1000	1341.6	164.9	1580.1	102.1	1.7	2.6

of fibers inner-structure as well as the resulting provision of higher electrical conductivity. As mentioned above, evolution of the nitrogen functional groups mainly happens in the temperature range from 750 °C to 900 °C, during which an amount of sp^2 domains is established, it may provide more active sites for the vanadium reaction and accelerate the reaction rate [41]. Compared with the 800 °C-carbonized nanofibres, the electrical conductivity of the 900 °C-carbonized nanofibres increases enormously, which will contribute to reduce the polarization and result in a superior electrochemical property [10,11,33]. As for the 1000 °C-carbonized nanofibres, the redox peaks current of the voltammogram is not improved further, while the peak potential separation becomes smaller still due to the further enhancement of the electrical conductivity.

3.7. Comparison with the TCFs

In order to compare the electrochemical property of the 1000 °C-carbonized nanofibres with that of TCFs, those two carbon fibers were used to modify the GCE and tested by CV at scan rate of 10 mV s^{-1} in the electrolyte containing 0.1 M $VOSO_4$ and 2 M H_2SO_4. The CV curves are shown in Fig. 10 and the electrochemical parameters are listed in Table 7. For the GCE, the oxidation peak of the VO^{2+}/VO_2^+ couple appears at 1.28 V while the corresponding reduction peak does not appear, implying that the conversion between VO^{2+} and VO_2^+ is quite irreversible. The anodic and cathodic peaks are centered at 1.13 V and 0.446 V for the GCE modified by TCFs, respectively. However, the peak potential separation is so large and the shape of two peaks is so asymmetric, indicating the

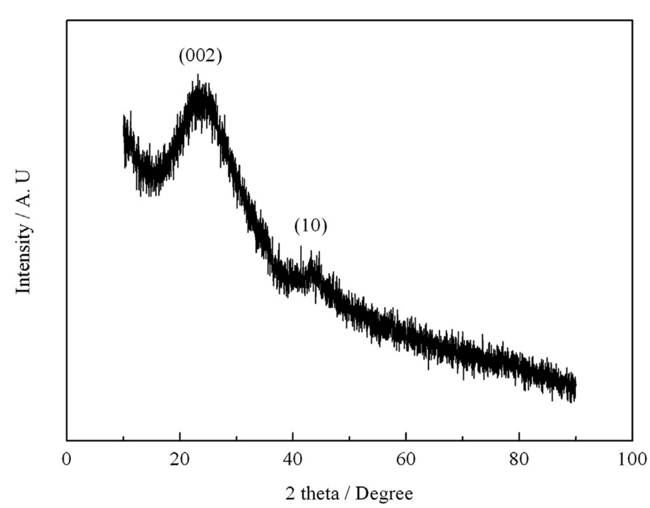

Fig. 6. XRD pattern of the 1000 °C-carbonized nanofibres.

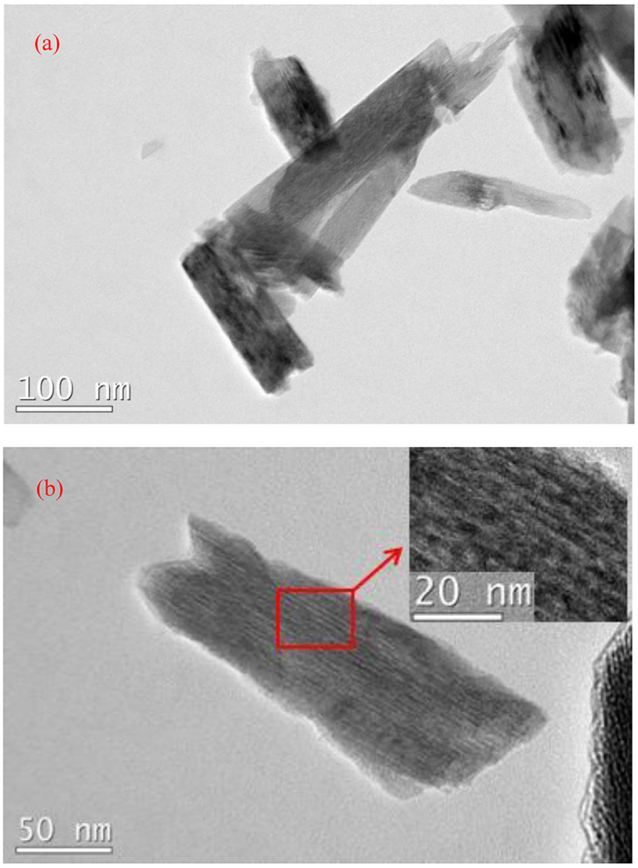

Fig. 7. TEM images of 1000 °C-carbonized nanofibres: (a) microstructure of the nanofibres at low resolution, (b) microstructure of the nanofibres at high resolution.

electrochemical property of the composite electrode is very poor. Compared to the former, the GCE modified by ECNFs present a higher electrochemical activity and better reversibility. Moreover, the lower oxidation potential (Ea = 0.970 V) of the sample implies a lower charge voltage for the VFB and a higher energy storage efficiency [42]. Since the diameter of the ECNFs is in range of 100–200 nm while that of the TCFs is about 20 um, thus, the graphite crystallites in the ECNFs will have more chance to be exposed to the

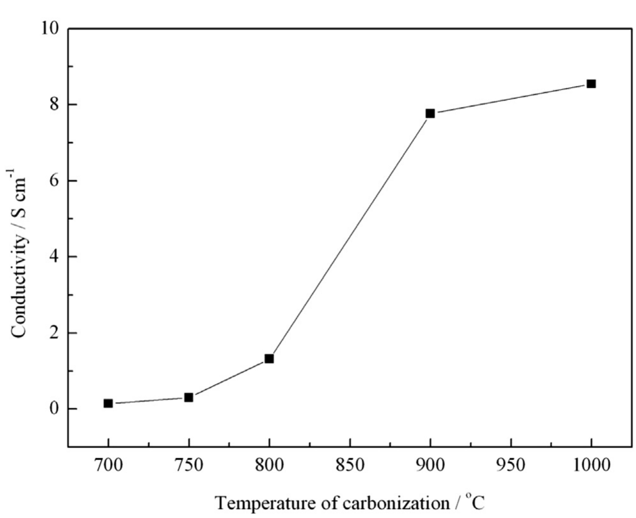

Fig. 8. Effect of the carbonization temperature on the electrical conductivity of the ECNFs.

Table 5
Electrical conductivity of the ECNFs at the different carbonization temperature.

Temperature (°C)	700	750	800	900	1000
Conductivity (S cm^{-1})	0.138	0.293	1.31	7.76	8.54

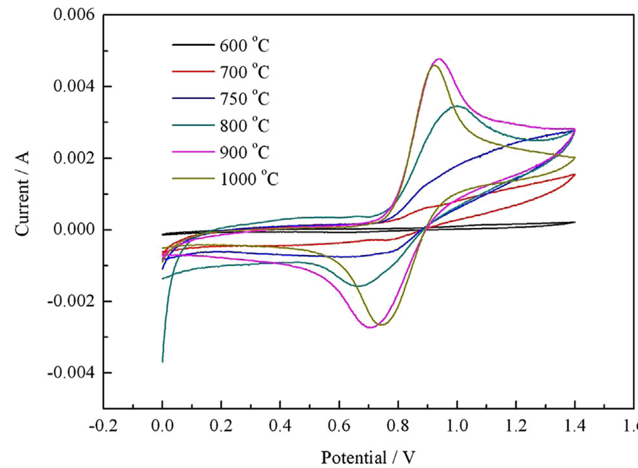

Fig. 9. CV curves for VO^{2+}/VO_2^+ couple on the ECNFs at the different carbonization temperature recorded at 2 mV s^{-1} scan rate in 0.1 M $VOSO_4$ + 2 M H_2SO_4.

Table 6
Parameters recorded by the CV curves for VO^{2+}/VO_2^+ couple on the ECNFs carbonized at the different temperature.

Temperature (°C)	Ipa (mA)	Ipc (mA)	−Ipa/Ipc	Ea (V)	Ec (V)	ΔEp (V)
800	3.46	−1.59	2.18	1.00	0.664	0.336
900	4.77	−2.74	1.74	0.938	0.710	0.228
1000	4.60	−2.66	1.73	0.924	0.744	0.180

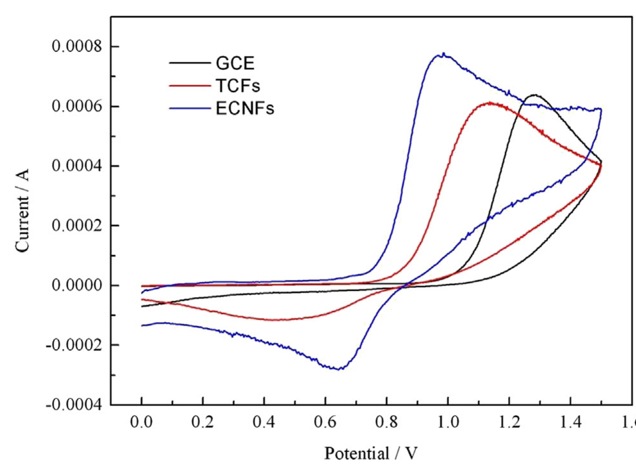

Fig. 10. CV curves for VO^{2+}/VO_2^+ couple on the GCE, TCFs and 1000 °C-carbonized nanofibres recorded at 10 mV s^{-1} scan rate in 0.1 M $VOSO_4$ + 2 M H_2SO_4.

Table 7
Parameters recorded by the CV curves for VO^{2+}/VO_2^+ couple on the GCE, GCE modified by TCFs and GCE modified by ECNFs.

Samples	Ipa (mA)	Ipc (mA)	−Ipa/Ipc	Ea (V)	Ec (V)	ΔEp (V)
GCE	0.639	–	–	1.28	–	–
TCFs	0.611	−0.116	5.27	1.13	0.446	0.684
ECNFs	0.771	−0.282	2.73	0.970	0.642	0.328

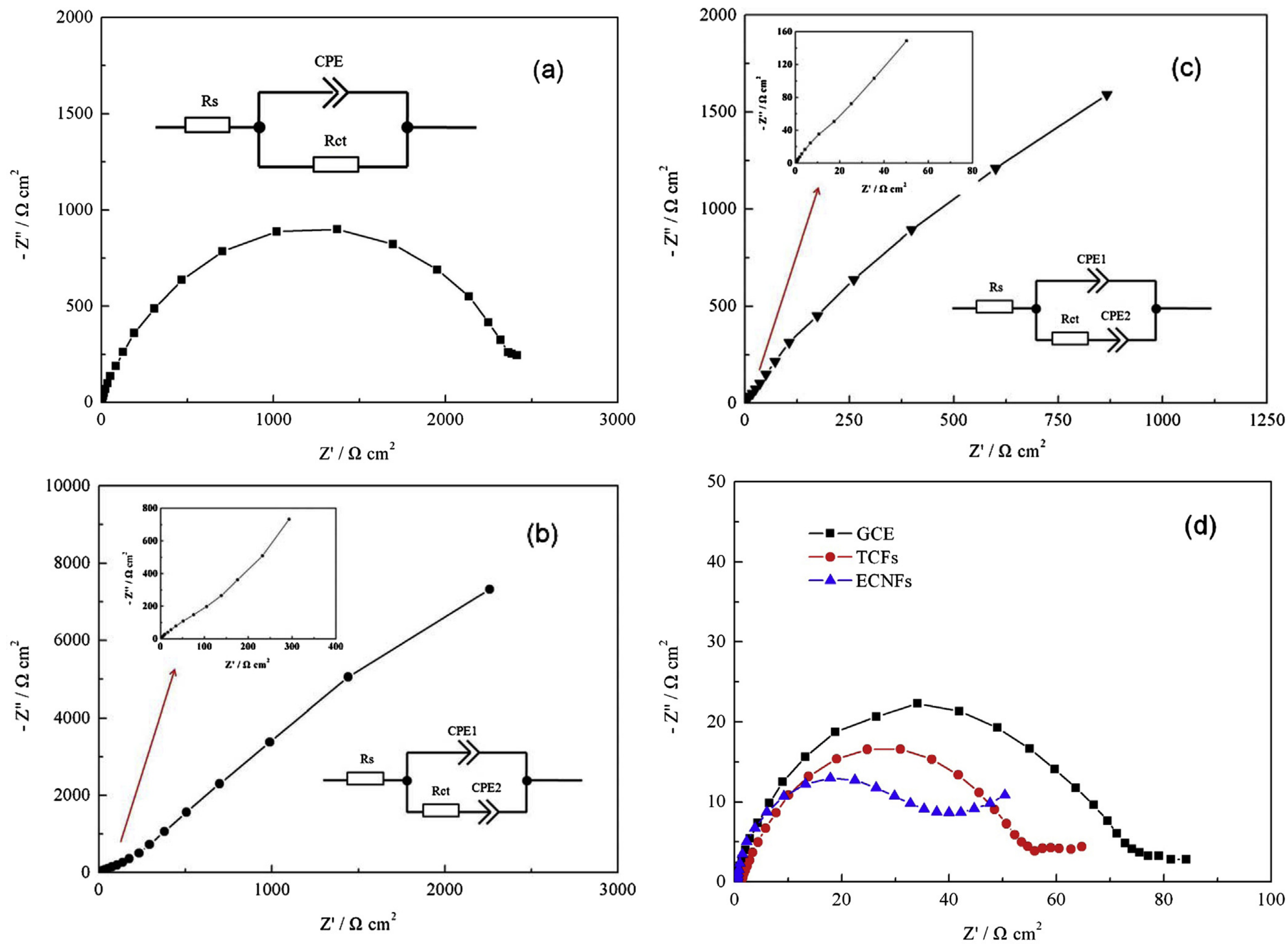

Fig. 11. Nyquist plots and the corresponding equivalent circuits of the three kinds of carbon materials in 0.1 M $VOSO_4$ + 2 M H_2SO_4 at different potentials: (a) GCE at the open-circuit potential, (b) GCE modified by TCFs at the open-circuit potential, (c) GCE modified by ECNFs at the open-circuit potential, (d) carbon materials at the polarization potential of 1 V.

surface of the carbon fibers. The surface defects and the exposed edges of the graphitic layers may facilitate the electron transfer and catalyze the vanadium reaction [9,39]. Furthermore, the ultrathin ECNFs possess much larger specific surface area than the TCFs. It can provide more suitable site for the vanadium reaction [43]. For the reasons mentioned above, the 1000 °C-carbonized nanofibres display better electrochemical performance than the TCFs.

In order to demonstrate the electrochemical behavior of the VO^{2+}/VO_2^+ couple on the carbon materials clearly, the EIS of them in the electrolyte containing 0.1 M $VOSO_4$ and 2 M H_2SO_4 were recorded at different potentials. The Nyquist plots and the corresponding equivalent circuits are illustrated in Fig. 11. As for the GCE modified by TCFs and the GCE modified by ECNFs, a semicircle and a linear part are observed in the frequency range from 10^5 Hz to 10^{-2} Hz at the open-circuit potential, indicating that the VO^{2+}/VO_2^+ redox reaction is mixcontrolled by charge transfer and diffusion steps. Nevertheless, the Nyquist plot of the GCE just includes a semicircle, indicating that the redox reaction on the GCE is only controlled by charge transfer step at the open-circuit potential. Thus, the Nyquist plots can be fitted with equivalent circuits in Fig. 11. In the equivalent circuits, Rs stands for the system ohmic resistance composed of the solution, electrode and the contact resistance, Rct represents the charge transfer resistance across the electrode/solution interface, CPE1 is the constant-phase element which represents the electric double-layer capacitance of electrode/solution interface, CPE2 is the constant-phase element which represents the diffusion capacitance attributed by the diffusion process of vanadium ions.

The parameters obtained from fitting the impedance plots with the equivalent circuits of Fig. 11 are listed in Table 8. According to the fitting result, the values of Rs for all of the carbon electrodes are in range of 0.1–0.4 Ω cm^2. Due to the micron level of the reaction current during the test, the IR drop value should be less than 10 mV. It can be seen that at the open-circuit potential, the charge transfer resistance decreases in the order of GCE, GCE modified by TCFs, GCE modified by ECNFs, conversely, one parameter of the constant-phase element Y_0 increases in the same order. The decrease of the Rct indicates that the electrochemical activity of the 1000 °C-carbonized nanofibres is better than that of TCFs. The increase of the $Y_{0,1}$ and $Y_{0,2}$ displays that the electric double-layer capacitance of the electrode/solution interface and the diffusion capacitance of vanadium ions for the ECNFs is larger than that of the TCFs. The

Table 8
Parameters obtained from fitting the impedance plots with the equivalent circuits of three kinds of carbon materials at the open-circuit potential.

Samples	Rs (Ω cm^2)	CPE1		Rct (Ω cm^2)	CPE2	
		$Y_{0,1}$	n		$Y_{0,2}$	n
GCE	0.185	1.54×10^{-4}	0.821	2401	–	–
TCFs	0.160	7.94×10^{-4}	0.805	578	5.32×10^{-4}	0.868
ECNFs	0.394	3.72×10^{-3}	0.863	319	9.44×10^{-4}	0.488

former favors the charge transfer for the VO^{2+}/VO_2^+ redox reaction and the latter is beneficial for the diffusion of vanadium ions. This is consistent with the CV result. In order to gain additional supporting evidence, the EIS characteristic of the three kinds of carbon materials at the polarization potential of 1 V is also obtained. The values of Rct for the GCE, GCE modified by TCFs and GCE modified by ECNFs are 73.2 Ω cm^2, 57.2 Ω cm^2, 22.4 Ω cm^2, respectively, which shows the same order as the result acquired at the open-circuit potential. As mentioned above, due to more active sites and larger specific surface area of the ECNFs, not only the charge transfer rate of the VO^{2+}/VO_2^+ redox reaction is promoted, but also the diffusion of vanadium ions is improved.

4. Conclusions

The ECNFs were firstly used as electrode materials for VFB in this paper. The effect of the carbonization temperature on the composition, structure, and properties of the ECNFs was investigated. The relationship between the inner-structure of the ECNFs and their properties was also studied. It is found that the diameters of the ECNFs are distributed with the range of 100–200 nm. The evolution of nitrogen functional groups mainly happens in the temperature range of 750–900 °C which results in greatly enhanced graphitization degree and huge improvement of the electrical conductivity. With the increasing of carbonization temperature, the electrochemical activities of carbon nanofibres toward the redox reaction of VO^{2+}/VO_2^+ couple are enhanced extensively. The 1000 °C-carbonized nanofibres show remarkable behavior among the samples and they also exhibit higher activity toward the vanadium reaction compared with the TCFs. The excellent performance of the ECNFs carbonized at higher temperature may attribute to the nanometer-sized diameter, forming of the 2-dimensional graphitic lattice and the improvement of the electrical conductivity.

Acknowledgments

This work is funded by National Basic Research Program of China (No. 2010CB227203).

References

[1] Z. Yang, J. Zhang, M.C.W. Kintner-Meyer, et al., Chem. Rev. 111 (2011) 3577–3613.
[2] F. Cheng, J. Liang, Z. Tao, et al., Adv. Mater. 23 (2011) 1695–1715.
[3] W. Wang, Q. Luo, B. Li, et al., Adv. Funct. Mater. 23 (2013) 970–986.
[4] Ch. Fabjan, J. Garche, B. Harrer, et al., Electrochim. Acta 47 (2001) 825–831.
[5] C.J. Rydh, J. Power Sourc. 80 (1999) 21–29.
[6] L. Joerissen, J. Garche, Ch. Fabjan, et al., J. Power Sourc. 127 (2004) 98–104.
[7] K.J. Kim, M.-S. Park, J.-H. Kim, et al., Chem. Commun. 48 (2012) 5455.
[8] C. Yao, H. Zhang, T. Liu, et al., J. Power Sourc. 218 (2012) 455–461.
[9] W. Li, J. Liu, C. Yan, Electrochim. Acta 56 (2011) 5290–5294.
[10] H.Q. Zhu, Y.M. Zhang, L. Yue, et al., J. Power Sourc. 184 (2008) 637–640.
[11] P. Han, Y. Yue, Z. Liu, et al., Energy Environ. Sci. 4 (2011) 4710.
[12] K.J. Kim, Y.-J. Kim, J.-H. Kim, et al., Mater. Chem. Phys. 131 (2011) 547–553.
[13] S. Wang, X. Zhao, T. Cochell, et al., J. Phys. Chem. 3 (2012) 2164–2167.
[14] B. Sun, M. Skyllas-Kazacos, Electrochim. Acta 37 (1992) 1253–1260.
[15] B. Sun, M. Skyllas-Kazacos, Electrochim. Acta 37 (1992) 2459–2465.
[16] L. Yue, W. Li, F. Sun, et al., Carbon 48 (2010) 3079–3090.
[17] W.H. Wang, X.D. Wang, Electrochim. Acta 52 (2007) 6755–6762.
[18] Z. González, A. Sánchez, C. Blanco, et al., Electrochem. Commun. 13 (2011) 1379–1382.
[19] C. Kim, K.S. Yang, Appl. Phys. Lett. 83 (2003) 1216.
[20] J. Li, E-h. Liu, W. Li, et al., J. Alloys Compd. 478 (2009) 371–374.
[21] L. Wang, Y. Yu, P.C. Chen, et al., J. Power Sourc. 183 (2008) 717–723.
[22] L. Zou, L. Gan, R. Lv, et al., Carbon 49 (2011) 89–95.
[23] S.N. Arshad, M. Naraghi, I. Chasiotis, Carbon 49 (2011) 1710–1719.
[24] Y. Yang, F. Simeon, T.A. Hatton, et al., J. Appl. Polym. Sci. 124 (2012) 3861–3870.
[25] J.R. Pels, F. Kapteijn, J.A. Moulijn, et al., Carbon 33 (1995) 1641–1653.
[26] C. Weidenthaler, A.-H. Lu, W. Schmidt, et al., Microporous Mesoporous Mater. 88 (2006) 238–243.
[27] S.D. Gardner, C.S.K. Singamsetty, G.L. Booth, Carbon 33 (1995) 587–595.
[28] S. Biniak, G. Szymanski, J. Siedlewski, Carbon 35 (1997) 1799–1810.
[29] Z.R. Yue, W. Jiang, L. Wang, et al., Carbon 37 (1999) 1785–1796.
[30] K. Láaszló, E. Tombácz, K. Josepovits, Carbon 39 (2001) 1217–1228.
[31] Y. Shao, X. Wang, M. Engelhard, et al., J. Power Sourc. 195 (2010) 4375–4379.
[32] C. Sheng, Fuel 86 (2007) 2316–2324.
[33] P. Han, H. Wang, Z. Liu, et al., Carbon 49 (2011) 693–700.
[34] F. Tuinstra, J. Chem. Phys. 53 (1970) 1126.
[35] D.S. Knight, W.B. White, Mater. Res. Soc. 4 (1989) 385–393.
[36] Y. Wang, S. Serrano, J.J. Santiago-Avilés, Synth. Met. 138 (2003) 423–427.
[37] B.-S. Lee, S.-B. Son, K.-M. Park, et al., J. Power Sourc. 199 (2012) 53–60.
[38] Z.Q. Li, C.J. Lu, Z.P. Xia, et al., Carbon 45 (2007) 1686–1695.
[39] Y. Qiu, J. Yu, T. Shi, et al., J. Power Sourc. 196 (2011) 9862–9867.
[40] E. Zussman, X. Chen, W. Ding, et al., Carbon 43 (2005) 2175–2185.
[41] Z. González, C. Botas, P. Álvarez, et al., Carbon 50 (2012) 828–834.
[42] C. Ponce de León, A. Frías-Ferrer, J. González-García, et al., J. Power Sourc. 160 (2006) 716–732.
[43] H.-M. Tsai, S.-Y. Yang, C.-C.M. Ma, et al., Electroanalysis 23 (2011) 2139–2143.